Supplementary Information

Lattice-Trapped Synthesis Enhances Fixation of As(V) in As@zeolite P

Lu Ma[1], Yu Li[1], Qi Wang[1], Ning Fen[1], Ruyang Wang[1], Mei Yang[1], Qian Ma[1] Yuanyuan Li[1], Yulong Ma[1], Yonggang Sun[1], Wenxin Ji[1*]

[1]State Key Laboratory of High-efficiency Utilization of Coal and Green Chemical Engineering, College of Chemistry and Chemical Engineering, Ningxia University, Yinchuan, China

*Corresponding author email: jwx@nxu.edu.cn

Text S1: Materials and methods

Text S2: DFT calculation details

Text S3: The study on the impact of contact time on removal kinetics and the removal isotherm

List of Figures and Tables

Fig. S1 shows the PXRD patterns of the CGCS.

Fig. S2 Model of zeolite P with immobilized As(V) for DFT calculations (a. Top view. b. Side view). Oxygen is shown in red, silicon in yellow, and aluminum in purple.

Fig. S3 Transmission electron microscopy (TEM) images of As@zeolite P.

Fig. S4 displays the structural information of the zeolite P (312) surface for DFT calculations. Oxygen is represented in red, silicon in yellow, and aluminum in purple.

Fig. S5 A illustrates the variation in the removal amount of $AsO_4^{3-}{}_{aq}$ on zeolite P at different contact times. B presents the relationship between the t/q_t of $AsO_4^{3-}{}_{aq}$ and time t. C: The plot of $In(q_e - q_t)$ of $AsO_4^{3-}{}_{aq}$ versus time t. D: The removal isotherm for $AsO_4^{3-}{}_{aq}$ by zeolite P. E: The leaching fixation rate of $As(V)_{aq}$ after removal by zeolite P under different pH conditions.

Fig. S6 The bond length data for the As-O tetrahedron and Si-O tetrahedron after optimization by DFT calculations are presented.

Table S1 XRF results of CGCS.

Table S2 Kinetic parameters for the removal of $AsO_4^{3-}{}_{aq}$ on zeolite P.

Table S3 Isotherm parameters for the removal of $AsO_4^{3-}{}_{aq}$ by zeolite P.

Table S4 Adsorption energies of AsO_4^{3-} ions on the zeolite P (312) surface. (ads, unit: kJ mol^{-1}）

Text S1: Materials and methods

1. Preparation of zeolite P

Firstly, 2 g of CGCS and 3 g of $Na_2SiO_3 \bullet 9H_2O$ were mixed uniformly and then ground in a mortar for 10 min. Subsequently, the mixture was transferred to a 50 mL hydrothermal reactor. The reaction was kept in a constant temperature oven at 80 ℃ for 48 h. After the reaction was completed, the product was thoroughly washed and then dried at 105 ℃ for 6 h. The dried samples are stored in a dryer for further characterization.

2. Removal of $As(V)_{aq}$ by Zeolite P

This study aims to investigate the removal behavior of Zeolite P towards $As(V)_{aq}$. Synthesized Zeolite P is added to arsenate solutions with concentrations ranging from 50 to 500 mg L^{-1}. Place the vials in a constant temperature oscillator at 150 rpm and 25 ℃. Pre-set sampling times are set at 30, 60, 360, 720, and 1440 min for kinetic experiments. Instantaneous arsenate concentrations are analyzed using a triple quadrupole inductively coupled plasma mass spectrometer (iCAP TQ ICP-MS, Thermo Scientific).

Text S2: DFT calculation details

In the computational study of the binding energy between AsO_4^{3-} anions and the pre-synthesized framework of As@zeolite P, the lattice parameters of zeolite P were initially set as a = 9.99 Å, b = 9.99 Å, c = 10.06 Å, and α = β = γ = 90°. To accommodate the analysis, a 2×1×1 supercell was constructed, resulting in a expanded unit cell with parameters a = 19.99 Å, b = 9.99 Å, c = 10.06 Å, and α = β = γ = 90°.

The Density Functional Theory (DFT) calculations for the interaction between AsO_4^{3-} and the zeolite P surface were performed using the DMol3 module within Materials Studio 2019. The calculations employed the DNP basis set and the GGA PBE exchange-correlation functional[1-6]. To ensure high computational precision, the convergence criteria were set to an energy threshold of 1.0×10^{-5} eV, a maximum force of 0.05 eV $Å^{-1}$, and a maximum displacement of 0.005 Å. The integration over the Brillouin zone of all surfaces was carried out using a 2×6×2 Monkhorst-Pack grid. For the zeolite P (3 1 2) surface, the principal parameters were refined to a = 28.38 Å, b = 9.99 Å, c = 37.27 Å, and α = β = γ = 90°.

To be more specific, first, build a box with 1 AsO_4^{3-} and zeolite P. In order to avoid the influence of other atoms, a vacuum layer with a thickness of 30 Å was added to the surface of zeolite P crystal. The zeolite P (312) surface is used in the calculation. All equilibrium structures are obtained without symmetry constraints. Additional details of the calculation are presented in text S1 in the support information. The adsorption energy ($E_{\mathrm{adsorption}}$) of $AsO_4^{3-}{}_{aq}$ onto the zeolite P (312) surface is calculated using Equation (4):

$$E_{ads} = E_{total} - E_{surface} - E_{arsenate\ anion} \quad (1)$$

here E_{total} is the total energy of zeolite P (312) crystal surface and AsO_4^{3-}, $E_{surface}$ is the total energy of zeolite P (312) crystal surface, $E_{arsenate\ anion}$ is the total energy of AsO_4^{3-}. Negative adsorption energy indicates that adsorption is exothermic; The more negative the adsorption energy is, the greater the absorption amount of adsorbent is. Fig. S4 and Table S2 show the structural information and adsorption energy of the zeolite P (312) surface for DFT calculations.

Text S3: The study on the impact of contact time on removal kinetics and the removal isotherm

To investigate the removal performance of zeolite P for $AsO_4^{3-}{}_{aq}$, a series of batch experiments were conducted. As shown in Fig. S5A, the contact time had a significant impact on the removal efficiency of $AsO_4^{3-}{}_{aq}$ by zeolite P. At the initial stage of the experiment, the removal rate increased rapidly and then entered a slow removal phase. As the contact time extended, the removal amount continued to increase until it reached an equilibrium state after approximately 30 min. The initial rapid removal phase could be attributed to the high availability of binding sites on the surface of zeolite P. Over time, these binding sites were gradually occupied and approached saturation, leading to a decrease in the removal rate in the later stage. This phenomenon is consistent with the reports of previous researchers, indicating that the removal process has similar dynamic characteristics.

This study further analyzed the variation of removal data over time using pseudo-first-order and pseudo-second-order kinetic models to provide deeper insights into the removal mechanism. The results show that within 30 min, the removal of $AsO_4^{3-}{}_{aq}$ by zeolite P had reached equilibrium, with the removal amount reaching a maximum, which provides an important basis for evaluating the equilibrium or maximum removal capacity. The models can be expressed as[7-9]:

Pseudo-first-order

$$In(q_e - q_t) = Inq_e - K_1 t \quad (1)$$

Pseudo-second-order

$$\frac{t}{q_t} = \frac{1}{K_2 q_e^2} + \frac{1}{q_e} t \quad (2)$$

where q_e (mg g^{-1}) and q_t (mg g^{-1}) respectively represent the amount of metal ions removed at equilibrium and at a specific time point. The rate constants K_1 (min^{-1}) and K_2 (g mg^{-1} min^{-1}) correspond to the kinetic parameters of the first-order and second-order removal models, respectively.

Table S2 presents the kinetic parameters calculated based on the two models. The parameter values for the pseudo-second-order model are higher than those for the pseudo-first-order model, indicating that the pseudo-second-order model has a higher fitting goodness in describing the removal kinetics of $AsO_4^{3-}{}_{aq}$ on zeolite P. Moreover, the relationship between the amount of $AsO_4^{3-}{}_{aq}$ removed and time (t/q_t vs. t curve) and the relationship between $In(q_e - q_t)$ and time t are shown in Fig. S5B and S5C, respectively. The results show that the t/qt vs. t curve further supports the validity of the pseudo-second-order model. Based on the assumption of the pseudo-second-order model, this study infers that the removal process of $AsO_4^{3-}{}_{aq}$ on zeolite P is primarily controlled by physical adsorption mechanisms and is closely related to diffusion processes. This inference is not only supported by the kinetic data but also aligns with the existing literature's understanding of similar removal systems.

The removal isotherm for $AsO_4^{3-}{}_{aq}$ removal by zeolite P is shown in Fig. S5D. The simulation of removal isotherms is generally performed using the Langmuir and Freundlich models, which can be expressed as[10]:

$$\frac{C_e}{q_e} = \frac{1}{q_{max} K_L} + \frac{C_e}{q_{max}} \quad (3)$$

$$logq_e = \frac{1}{n} logC_e + logK_F \quad (4)$$

where C_e (mg L^{-1}) is the equilibrium concentration of the metal ions in the solution, q_e (mg g^{-1}) and q_{max} (mg g^{-1}) are the equilibrium removal amount and the maximum removal capacity, respectively, K_L (L mg^{-1}) is the constant of the Langmuir isotherm, and K_F and n are the constants of the Freundlich isotherm.

Table S3 details the related parameters of the Langmuir and Freundlich isotherm models. The data from Table S3 show that after comparing the coefficient of determination (R^2) of the two models, the Langmuir model provides a higher fitting degree for the removal behavior of $AsO_4^{3-}{}_{aq}$. According to the Langmuir isotherm model, the maximum removal capacity for $AsO_4^{3-}{}_{aq}$ is 14.08 mg g^{-1}. Additionally, the results shown in Fig. S5E indicate that under strongly alkaline conditions at a pH of 12, the fixation rate of $AsO_4^{3-}{}_{aq}$ is relatively low (86.68%), suggesting the leaching of $AsO_4^{3-}{}_{aq}$ from zeolite P in highly alkaline environments.

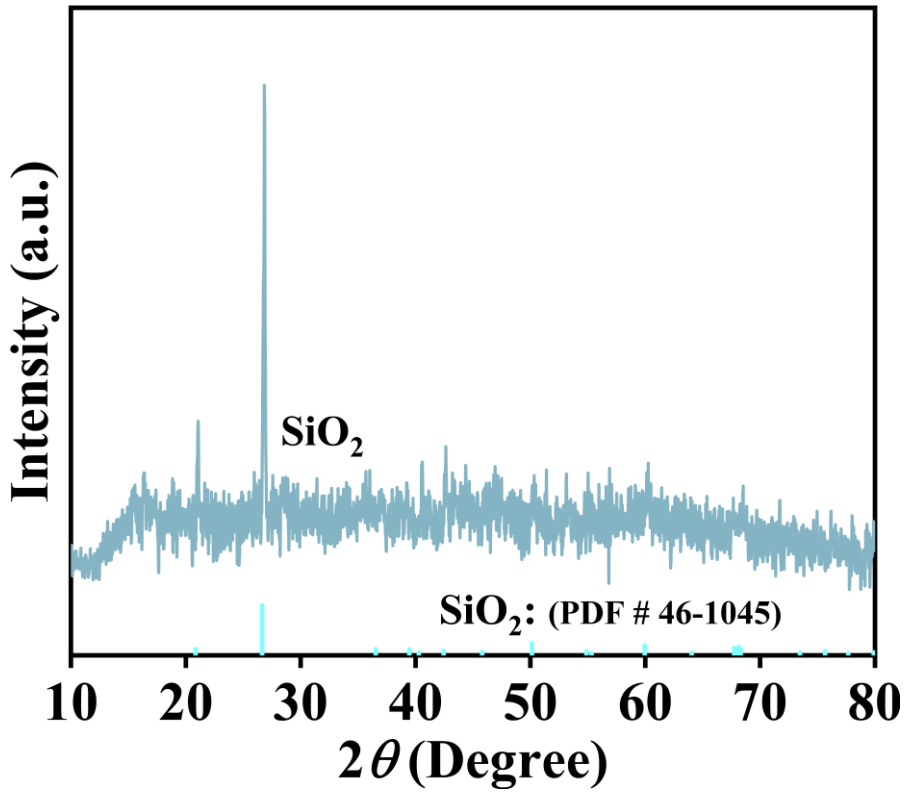

Fig. S1 Shows the PXRD patterns of the CGCS.

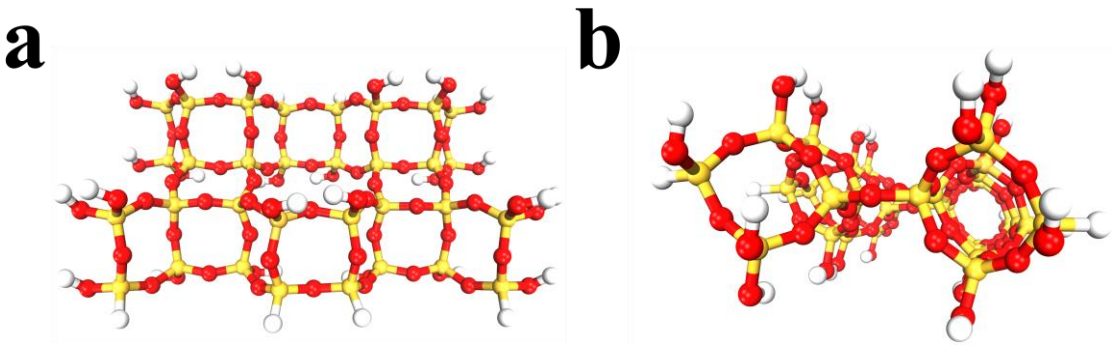

Fig. S2 Model of zeolite P with immobilized As(V) for DFT calculations (a. Top view. b. Side view). Oxygen is shown in red, silicon in yellow, and aluminum in purple.

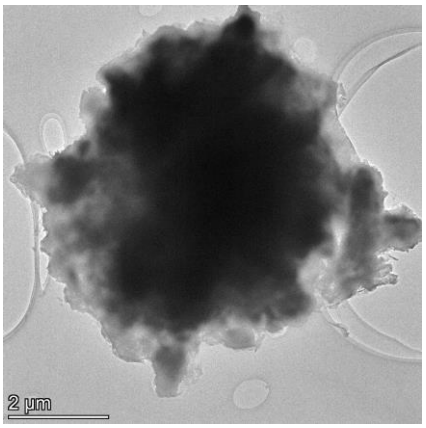

Fig. S3 Transmission electron microscopy (TEM) images of As@zeolite P.

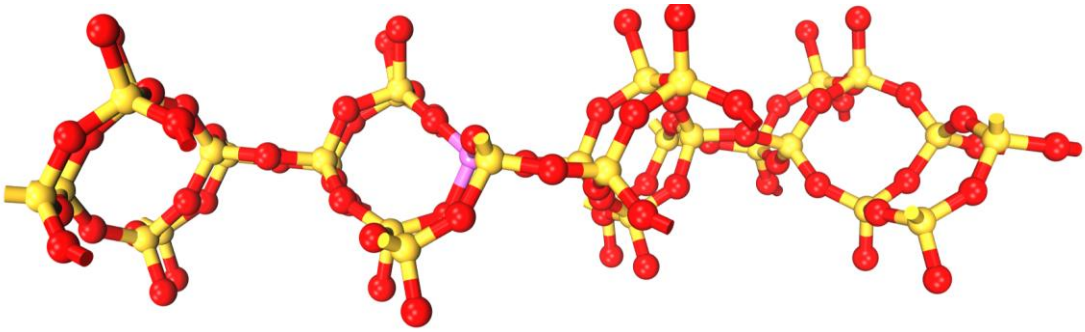

Fig. S4 Displays the structural information of the zeolite P (312) surface for DFT calculations. Oxygen is represented in red, silicon in yellow, and aluminum in purple.

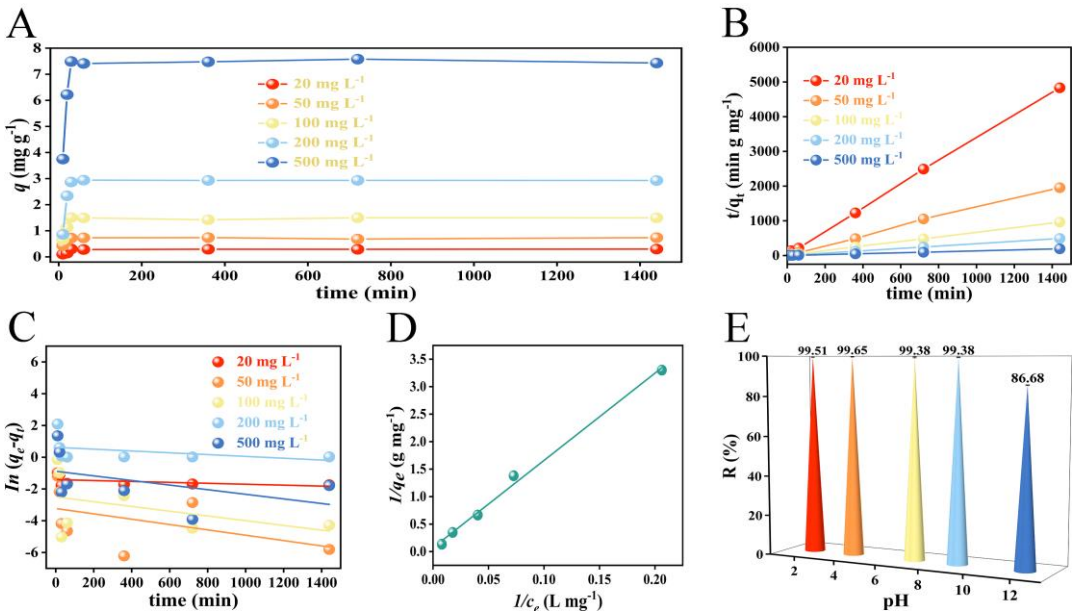

Fig. S5 A illustrates the variation in the removal amount of $AsO_4^{3-}{}_{aq}$ on zeolite P at different contact times. B presents the relationship between the t/q_t of $AsO_4^{3-}{}_{aq}$ and time t. C: The plot of $In(q_e - q_t)$ of $AsO_4^{3-}{}_{aq}$ versus time t. D: The removal isotherm for $AsO_4^{3-}{}_{aq}$ by zeolite P. E: The leaching fixation rate of $As(V)_{aq}$ after removal by zeolite P under different pH conditions.

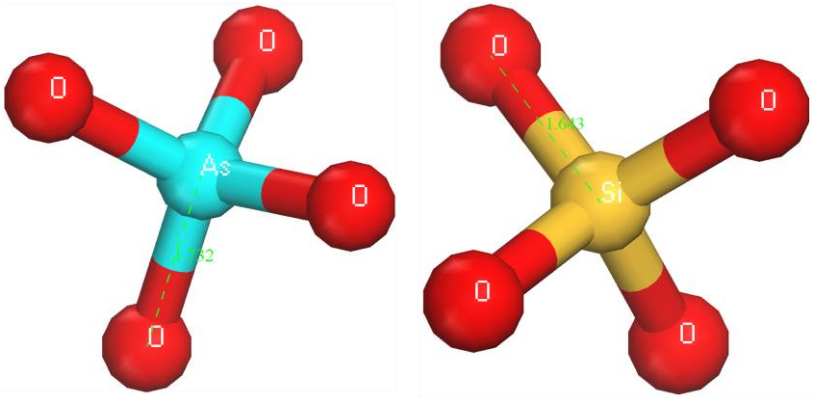

As-O 1.73 Å **Si-O 1.64 Å**

Fig. S6 The bond length data for the As-O tetrahedron and Si-O tetrahedron after optimization by DFT calculations are presented.

Table S1 XRF results of CGCS

Oxides	SiO_2	Al_2O_3	Na_2O	Fe_2O_3	MgO	CaO	K_2O	TiO_2
Wt.%	53.11	19.72	1.80	8.61	2.46	8.97	2.42	1.05

Table S2 Kinetic parameters for the removal of AsO_4^{3-}aq on zeolite P

Pseudo-first-order					Pseudo-second-order		
C_0 (mg L^{-1})	$k_1 \times 10^{-4}$ (min^{-1})	$q_{e,cal}$ (mg g^{-1})	R^2	$q_{e,exp}$ (mg g^{-1})	k_2 (mg g^{-1} min^{-1}	R^2	$q_{e,cal}$ (mg g^{-1})
20	2.91	0.245	0.228	0.30	0.27	0.999	0.30
50	16.80	0.400	0.233	0.72	0.22	0.999	0.73
100	14.90	0.083	0.178	1.50	0.10	0.999	1.49
200	5.70	1.856	0.157	2.87	0.05	0.999	2.94
500	14.50	0.416	0.200	7.49	0.07	0.999	7.69

Table S3 Isotherm parameters for the removal of AsO_4^{3-}aq by zeolite P

Isotherms	Parameters	$AsO_4^{3-}{}_{aq}$
Langmuir	q_{max} (mg g^{-1})	14.08
	K_L (L mg^{-1})	0.004
	R^2	0.995
Freundlich	K_F	0.061
	$1/n$	0.980
	R^2	0.994

Table S4 Adsorption energies of AsO_4^{3-}aq ions on the zeolite P (312) surface. (ads, unit: kJ mol^{-1})

E_{total}	$E_{surface}$	$E_{arsenate\ anion}$	E_{ads}
-17177.12	-14639.90	-2537.20	-10.37

References

1. G. Kresse and J. Hafner, *J Phys-Condens Mat*, 1994, **6**, 8245.
2. G. Kresse and J. Furthmüller, *Phys Rev B*, 1996, **54**, 11169-11186.
3. G. Kresse and J. Furthmüller, *Comp Mater Sci* , 1996, **6**, 15-50.
4. G. Kresse and J. Hafner, *Phys Rev B*, 1993, **47**, 558-561.
5. G. Kresse and D. Joubert, *Phys Rev B*, 1999, **59**, 1758-1775.
6. J. Gao, Y. Zheng, J.-M. Jehng, Y. Tang, I. E. Wachs and S. G. Podkolzin, *Science*, 2015, **348**, 686-690.
7. Y. Niu, W. Hu, M. Guo, Y. Wang, J. Jia and Z. Hu, *Carbohyd Polym*, 2019, **225**, 115218.
8. Y. Yang, Y. Wang, C. Xue, Y. Lin, J.-F. Lee, X. Yi and Z. Dang, *J Clean Prod*, 2024, **452**, 141936.
9. L. Chi, C. Huang, Z. Li, S. Ruan, B. Peng, M. Li, Q. Liang, K. Yin and S. Lu, *Cem Concr Compos*, 2024, **152**, 105667.
10. G. Z. Kyzas, G. Bomis, R. I. Kosheleva, E. K. Efthimiadou, E. P. Favvas, M. Kostoglou and A. C. Mitropoulos, *Chem Eng J*, 2019, **356**, 91-97.